NASA TECHNICAL NOTE

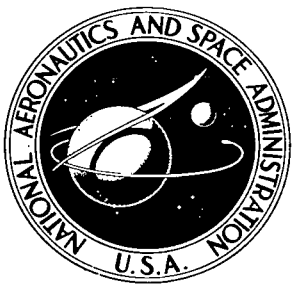

NASA TN D-5356

NASA TN D-5356

THE USE OF ENERGY THICKNESS IN PREDICTION OF THROAT HEAT TRANSFER IN ROCKET NOZZLES

by Robert W. Graham and Donald R. Boldman

Lewis Research Center
Cleveland, Ohio

NATIONAL AERONAUTICS AND SPACE ADMINISTRATION • WASHINGTON, D. C. • JULY 1969

THE USE OF ENERGY THICKNESS IN PREDICTION OF THROAT HEAT TRANSFER IN ROCKET NOZZLES

By Robert W. Graham and Donald R. Boldman

Lewis Research Center
Cleveland, Ohio

NATIONAL AERONAUTICS AND SPACE ADMINISTRATION

For sale by the Clearinghouse for Federal Scientific and Technical Information
Springfield, Virginia 22151 – CFSTI price $3.00

ABSTRACT

Boundary layer profile measurements in the convergent portion of a convergent-divergent nozzle have verified that the thermal layer is much thicker than the velocity layer. This observation supports the use of the integral energy boundary layer analysis in estimating heat transfer at the throat of a nozzle. An approximate integral-energy method is proposed which will enable gas-side, throat heat transfer predictions to be made without the aid of a large computer. The method has been tested over a range of nozzle geometries (area contraction ratios, 4 to 19) and temperature ratios (wall to gas ratios from 0.25 to 0.85).

THE USE OF ENERGY THICKNESS IN PREDICTION OF THROAT HEAT TRANSFER IN ROCKET NOZZLES

by Robert W. Graham and Donald R. Boldman

Lewis Research Center

SUMMARY

Boundary layer profile measurements in the convergent portion of a convergent-divergent nozzle have verified that the thermal layer is much thicker than the velocity layer. This observation supports the use of the integral energy boundary layer analysis in estimating heat transfer at the throat of a nozzle. An approximate integral-energy method is proposed which will enable gas-side, throat-heat transfer predictions to be made without the aid of a large computer. The method has been tested over a range of nozzle geometries (area contraction ratios, 4 to 19) and temperature ratios (wall to gas ratios from 0.25 to 0.85).

INTRODUCTION

Recent studies of heat transfer in rocket-type nozzle configurations have pointed to the importance of the behavior of the thermal boundary layer in evaluating the heat transfer rates, particularly at the throat and convergent portion of the nozzle. For instance, it was shown in references 1 and 2 that when the upstream thermal and velocity boundary layer histories were varied, the thermal boundary layer was the primary influence in establishing the level of heat transfer at the throat station.

In reference 1, an integral energy technique was presented which was a modification and simplification of the integral momentum and energy technique of reference 3. The simplified method was observed to produce local heat-transfer predictions which were comparable to the more complicated boundary layer analysis of reference 3, where the interaction exponent n was zero. (The interested reader should examine reference 3 in more detail, where the interaction coefficient was introduced to correct for unequal thicknesses of the thermal and velocity boundary layers.) Thus, the authors of reference 1 suggested that the simplified integral energy technique could be used in place of the method of reference 3. Also it was shown in reference 1 that the integral energy

method gave (for condition where ref. 3 interaction exponent n = 0) the best agreement with experimental heat transfer data at the throat of air nozzles. Such agreement has inferred that the thermal layer is much thicker than the velocity layer and the thermal layer thickness is the important boundary layer dimension for correlation of heat transfer data.

In general, it does seem plausible to select an integral energy approach for physical situations in which the **thermal layer** is thicker than the velocity layer. The heat transfer to low Prandtl number fluids in a channel entrance region is an example where the thermal layer is thicker than the velocity layer and where an energy approach is applicable (refs. 4 and 5). As will be shown herein, the subsonic and sonic portions of a converging-diverging nozzle satisfy the criteria for the integral energy method application.

In further support of the application of integral energy method to nozzles, several new pieces of evidence will be presented herein. First, experimental measurements of the thermal layer energy thickness will be presented and compared to the momentum thickness for the converging and diverging portions of C-D air nozzles. These experimental thickness values will be compared to boundary layer analysis estimates of the energy thicknesses. In particular, the energy thicknesses obtained from the integral method of reference 3 will be compared with the experimental data.

In addition, the integral energy method of reference 1 will be further simplified such that the energy thickness distribution in the nozzle can be easily estimated. Such a method will enable rapid design-type estimates of local heat transfer rates to be made, and will be more accurate than the standard forced convection correlations used in design estimates. The nozzle throat will be the station of greatest concern. The merits of this design approach will be tested by comparing its output with both experimental measurements and boundary layer calculations. The experimental measurements will encompass air nozzle and chemical rocket data for a range of geometries. The method is applicable only to the turbulent conditions associated with large Reynolds numbers ($Re_d \approx 10^6$) and does not apply to the laminar-like detransition observed when the momentum thickness Reynolds number is less than 360 (see ref. 6). Laminar flow nozzle heat transfer calculations can be applied to this peculiar regime resulting in satisfactory predictions of the throat heat transfer.

In support of the energy integral method, a model of the thermal layer for accelerated flow will be discussed. A qualitative discussion of the effects of acceleration on the transport mechanism will be included.

SYMBOLS

A area

d local diameter

h heat transfer coefficient

l inlet length

M Mach number

n interaction exponent (ref. 3)

P pressure

Pr Prandtl number

Re Reynolds number

S distance along wall (subsonic nozzle)

$\overline{S}$ distance along wall (supersonic nozzle)

St Stanton number

T temperature

u velocity

x axial distance from nozzle throat

y distance from wall

Z axial distance from nozzle entrance

α nozzle contraction angle

Δ thermal boundary layer thickness

δ velocity boundary layer thickness

θ momentum thickness

μ dynamic viscosity

φ energy thickness

Subscripts:

d based on diameter

e boundary layer edge condition

fd fully developed boundary layer

i inlet, refers to nozzle generally

r based on a reference temperature

t local stagnation condition

th throat condition

w wall condition

0 plenum condition

∞ free stream condition or based on an integration to free stream conditions.

APPARATUS

The local heat transfer data and boundary layer measurements employed in the analytical comparisons of this report were obtained chiefly from heated air investigations with conical nozzles. In addition to the air investigations, a more limited amount of measured local heat transfer data exists for rocket firings. The high temperature of the gases of the rocket firing have prevented any boundary layer surveys from being made in these rocket tests.

Since the heated air data provided an extensive base of conditions and geometries, it was the principal source of comparison. The heated air apparatuses referenced comprised:

(1) A heat exchanger or burner for elevating the temperature of the air

(2) An inlet plenum or calming chamber

(3)An entrance duct for introducing the air into the nozzle

(4) A water-cooled nozzle which was instrumented for the measurement of local heat transfer

(5) An exhaust system

A schematic of the heated air facility located at the Lewis Research Center is shown in figure 1. A more complete description of this facility can be found in references 1 and 2.

The instrumentation involved in the experiments included transient or steady-state heat flux meters and pressure and temperature boundary layer probes. Transient heat flux meters were employed in the chemical rocket tests (ref. 7) and steady-state heat flux meters for the heated air experiments. Boundary layer probes were utilized in the heated-air experiments only. For complete details on the instrumentation, the reader is referred to the original reports (refs. 1, 2, 6, and 7). The boundary layer surveys of the temperature layer are particularly important with regard to the application of the integral energy method discussed herein. Consequently, a sketch of the temperature probe is shown in figure 2. A similar type probe is described in reference 2. The probe is a 0.003 inch (0.076 mm) diameter open ball junction Chromel-Alumel thermocouple assembly encased in a conical afterbody which is brazed to a cylindrical strut. The entire probe was mounted in a precision actuator so that it could be traversed remotely through the boundary layer region. The recovery factor for the probe was determined from calibrations.

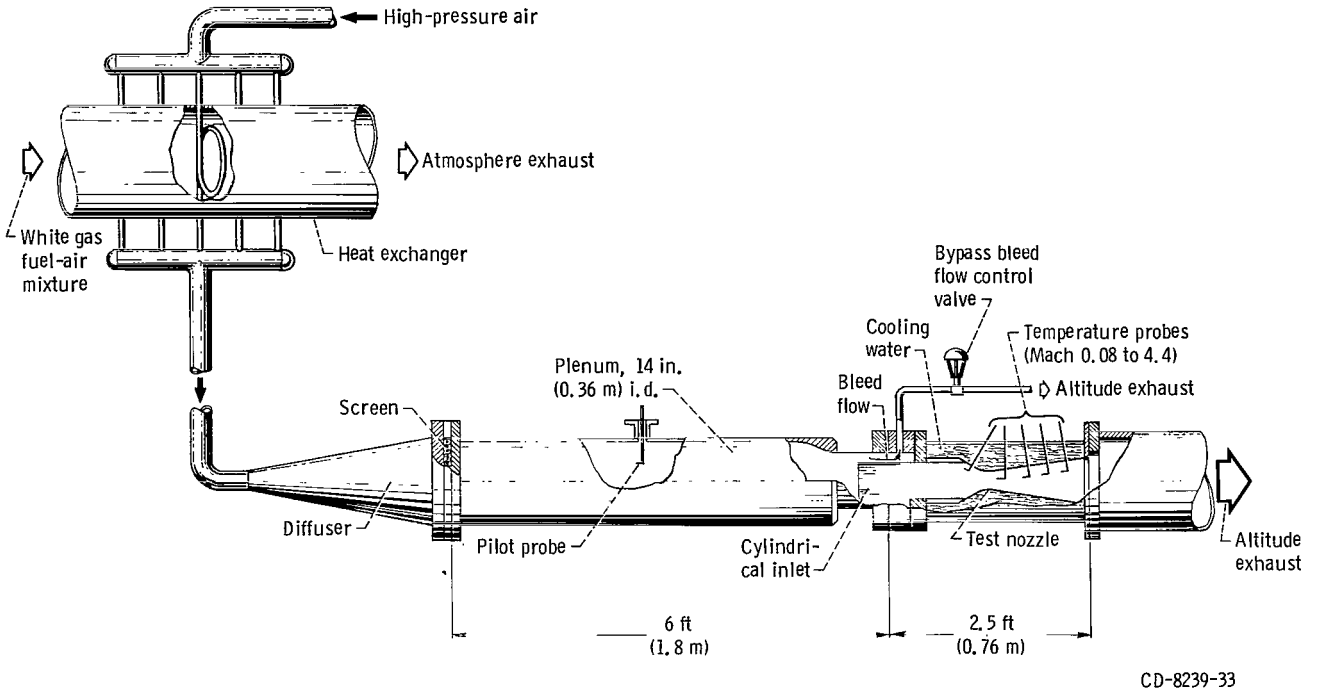

Figure 1. - Schematic diagram of nozzle heat transfer facility.

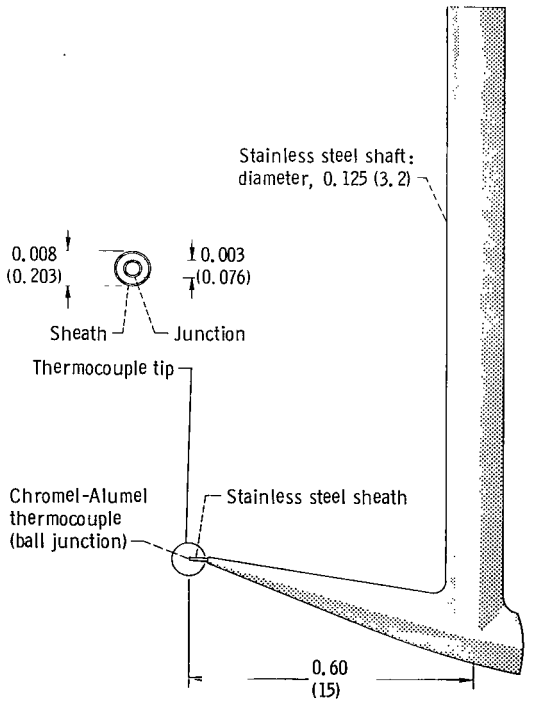

Figure 2. - Boundary layer temperature probe. All dimensions are in inches (mm).

RESULTS

The experimental results, especially the local heat transfer rates, utilized in this report have, for the most part, been published. The principal exception is some of the boundary layer survey information obtained in heated air tests, which is important to the establishment of certain assumptions in the analytical method presented herein.

Boundary Layer Measurements

Temperature and velocity boundary layer thicknesses based on profile data will be presented for several axial stations in the air nozzle. The stations of interest are designated according to the free stream Mach number at the axial station where the boundary layer surveys were made. The stations are M = 0.08, 1.3, 2.1, 3.7, and 4.4. The station associated with M = 1.3 will be designated at the throat station. This station was as close to the physical throat as could be realized without experiencing severe probe blockage effects. The throat station was the only station where no velocity boundary layer surveys were taken. The extreme thinness of the layer prevented such surveys, although temperature surveys were possible. All of the measurements reported herein were made at the Lewis Research Center air facility with a 30° half-angle convergence and 15° half-angle divergence nozzle.

Figures 3(a) and (b) are the energy layer and momentum layer thickness distributions in the nozzle for adiabatic and cooled inlet pipe entrance sections, respectively. The energy thickness discussed herein is defined as

$$\varphi = \int_0^{\Delta} \frac{\rho u}{(\rho u)_e} \left(1 - \frac{T_t - T_w}{T_{t,e} - T_w}\right) dy \tag{1}$$

The momentum thickness is

$$\theta = \int_0^{\delta} \frac{\rho u}{(\rho u)_e} \left(1 - \frac{u}{u_e}\right) dy \tag{2}$$

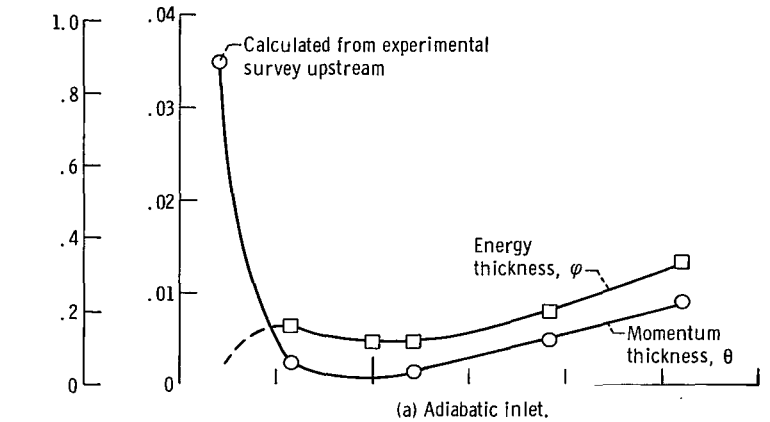

(a) Adiabatic inlet.

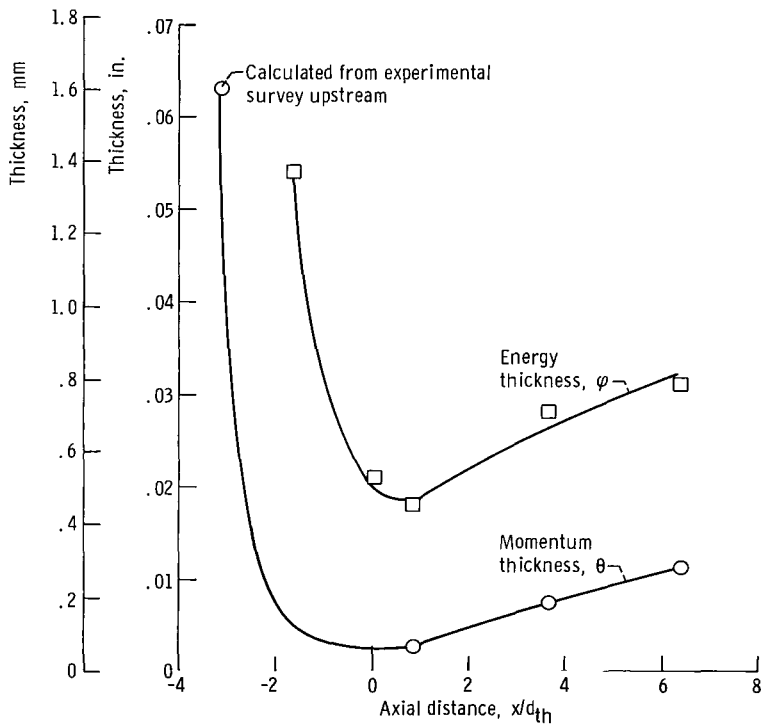

(b) Cooled inlet.

Figure 3. - Experimental integral boundary layer thickness along 30°-15° half-angle convergent-divergent nozzle. Inlet diameter, 6.5 inches (0.165 m); throat diameter, d_{th}, 1.492 in. (3.790 cm).

Since profile measurements of the velocity boundary layer were not possible at the throat, the momentum thickness there was extrapolated from upstream data by a boundary layer calculation.

It is obvious from figures 3(a) and (b) that downstream of the nozzle entrance, the energy thickness becomes greater than the momentum thickness. This condition persists downstream past the throat into the supersonic region. If one examines the momentum equation, an explanation for this behavior is quite apparent. In the subsonic and near-sonic region, the acceleration term in the momentum equation is much larger than the wall shear term. However, the dominance of the acceleration term dies away when the flow becomes supersonic and shear becomes important again.

The large thermal or energy layer thickness as compared to the momentum thickness in the subsonic and sonic sections of the nozzle, supports the applicability of an integral energy approach for these stations.

Comparison of figures 3(a) and (b) lends further support to the importance of thermal layer history. The thermal history introduced by the cooled inlet pipe greatly affects the local thermal thickness. It is particularly significant to compare the throat values of the two figures.

Further evidence for the importance of history can be observed from the temperature boundary layer profiles themselves. In figure 4, the temperature profile data for the throat station are plotted on logarithmic coordinates (temperature against distance) for

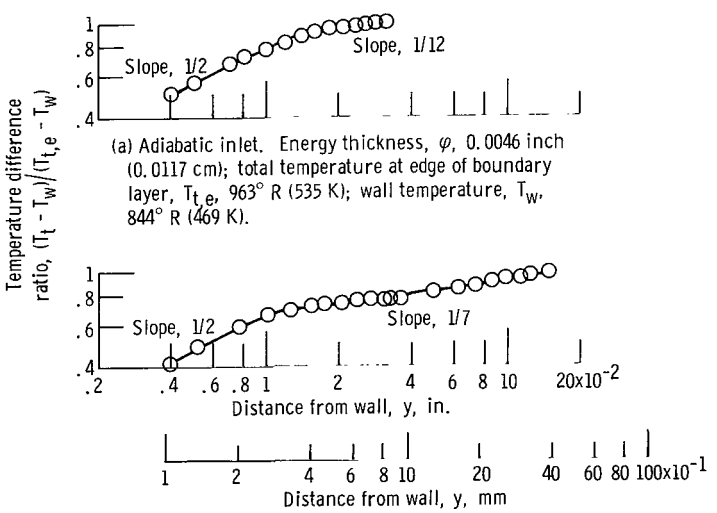

Figure 4. - Thermal boundary layer near throat at Mach 1.3. 30° half-angle of convergence nozzle. Inlet diameter, 6.5 inches (0.165 m).

the adiabatic and cooled pipe inlet. Plotting the data in this manner helps to bring out the exponential relation between temperature and radial distance. Note that the data for the throat station show distinctive breaks in the slopes, but where these changes occur varies between the adiabatic and cooled inlets. For instance both profiles appear to follow a slope of one-half near the wall. However, in the case of the cooled inlet the slope changed to the conventional turbulent value of 1/7 at a distance $y \approx 10^{-2}$ inch (0.25 mm) while for the adiabatic inlet, the slope changed to about 1/12 at a distance $y \approx 1.5 \times 10^{-2}$ inch (0.38 mm). For the cooled inlet, the profile exponent of 1/7 is interpreted to represent the residue of the thermal profile that was developed in the inlet pipe to the nozzle. Thus, the cooled inlet upstream of the nozzle has a marked effect on both the shape and thickness of the thermal boundary layer at the throat.

Judging from the variation in the slopes of the temperature profiles, the traditional use of the 1/7 exponent should be questioned. It appears that a more realistic average value would be closer to 1/4 for accelerated temperature boundary layers at the throat station. Profile data not shown here indicate that the 1/4 exponent pertains to the supersonic divergent portion of the nozzle also. However, it must be pointed out that the selection of the edge thickness has considerable bearing on the value of the exponent used.

Heat Transfer

Figures 5(a) and (b) show the experimental values of heat transfer at two nozzle stations for an adiabatic and cooled pipe inlet to the nozzle. The two stations are the throat and the station corresponding to $M = 0.08$. The nozzle is the 30° half-angle conic with an area contraction ratio of 19. The heat-transfer results for the adiabatic inlet at high Reynolds number have been published and discussed before in reference 1. The results for tests with the cooled inlet have been presented in reference 6. When the coordinates of $StPr^{0.7}$ and $Re_{d,r}$ are used, it is clear that two distinctive regimes of heat transfer are present. There is a "turbulent" level and a "laminar" level of $StPr^{0.7}$ which is particularly obvious for the throat data. The dramatic dropoff in the throat heat transfer below Reynolds numbers of a approximately 10^6 has been labeled "laminarization" of the heat transfer. (The reader is directed to ref. 6 for a more complete discussion of the phenomenon and a list of references.)

The simplified analysis to be presented in this report is directed to the turbulent level regime. Only mention will be made of laminar analyses in dealing with that level of heat transfer. Calculations not presented herein do indicate that the analysis presented in reference 8, for example, predicts the laminar-like level of heat transfer for the throat station shown in figure 5. However, these predictions do not seem to differ greatly from those obtained from laminar flat plate correlations. This is quite different from the com-

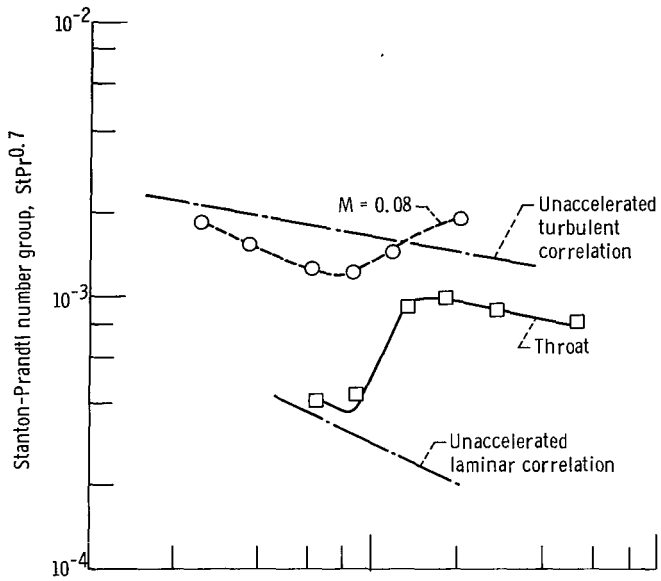

(a) Adiabatic inlet.

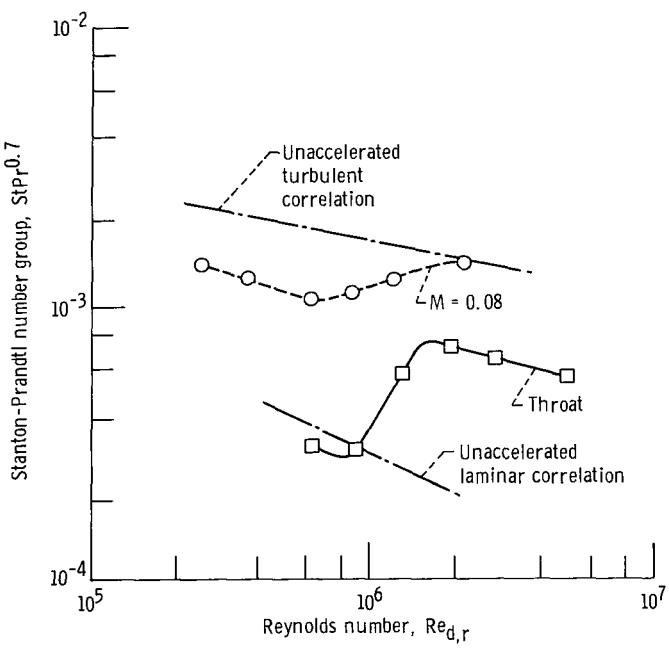

(b) Cooled inlet.

Figure 5. - Local heat transfer at Mach 0.08 and throat for heated air. Free-stream total temperature, T_0, 970° R (539 K); 30° half-angle convergence nozzle; inlet contraction ratio, 19.

parison made between data and flat plate correlation in the turbulent regime. For the turbulent level, the experimental values of heat transfer are appreciably below turbulent flow predictions of unaccelerated flow. The ability of a simplified energy integral technique to comprehend this decrement in heat transfer will be demonstrated in a later section.

Model of Thermal Layer

In an earlier section dealing with experimental results, the thermal boundary layer was shown to be thicker than the velocity layer. In fact, approximately an order of magnitude separates the two thicknesses for much of the subsonic and sonic domain (see fig. 3). As has been stated before, this observation is the basis for justifying an energy approach to the computation of heat transfer in these regions. For a fluid that has a Prandtl number of near unity, the occurrence of a thermal layer which is much thicker than the velocity layer may be classed as nonconventional. (For fluids with low Prandtl numbers, thick thermal layers are expected.) Therefore a discussion of a model of the thermal boundary layer for accelerated flow is warranted.

One way of looking at the accelerated thermal boundary layer is to consider it to be made up of two regions as shown in figure 6. A region near to the wall exists which corresponds to the thickness of the velocity boundary layer. (The eddy structure of the velocity boundary layer is sensed in the temperature layer.) Acceleration effects, which are

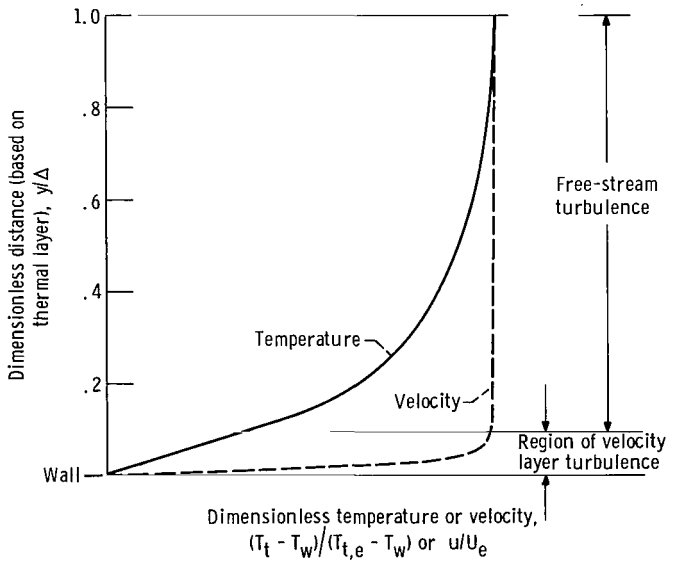

Figure 6. - Schematic of velocity and temperature boundary layers showing relative thicknesses for accelerating flow near throat.

known to attenuate the intensity of the turbulence in the velocity layer, will influence the transport phenomena in the thermal layer. What is being said here is that despite the difference in the boundary layer thicknesses, an important eddy transport interaction exists between the two layers for the near-wall region.

The second region of the thermal layer, shown in figure 6, is the larger outer region which reaches into the constant velocity or free stream flow of the nozzle. Intuitively, the turbulence structure of the free stream could influence turbulent transport in this part of the thermal layer.

The literature has dealt with acceleration effects in each of these regions. In references such as 2, 9, and 10, it was concluded that the turbulent structure within the boundary layer was attenuated by the acceleration.

Acceleration effects on the free stream turbulent structure would probably be related to studies of the behavior of weak, homogeneous turbulence under conditions of strain and shear. Such analytical studies have been carried on by Deissler (ref. 11). The free stream region depicted in figure 6 is a region of zero shear (no velocity gradient in normal direction). The effect of strain (acceleration) is a diminution in the intensity of turbulence. It turns out that the components of the fluctuating velocities remain about constant in magnitude when subjected to acceleration; the reduction in intensity results from an increased average free stream velocity. In reference 12, it was reported that the reduction in heat transfer due to acceleration observed in reference 9 could be approximated by the calculated reduction in the free stream turbulence intensity.

Thus, in both segments of the thermal boundary layer, acceleration appears to produce reductions in heat transport.

Consideration of the thermal transport in the free stream region does raise a significant question. For the unaccelerated turbulent boundary layers with gases, we normally associate the temperature gradient with a velocity gradient. Furthermore, by Reynolds analogy, the thermal eddy diffusivity and momentum eddy diffusivity are equivalent. These diffusivities are defined as

$$\epsilon_h = - \frac{\overline{t'v'}}{\frac{dT}{dy}} \qquad \text{(Thermal)}$$

$$\epsilon_m = - \frac{\overline{u'v'}}{\frac{du}{dy}} \qquad \text{(Momentum)}$$

In the free stream portion of the thermal layer, no gradient exists, yet a temperature gradient was measured. Does this mean that there is no eddy transport of heat in this portion? The answer is thermal diffusivity does exist! Such a conclusion can be obtained from the literature dealing with the statistical nature of turbulence. In reference 11, Deissler showed that finite values of diffusive heat transfer do exist for zero shear over a range of accelerations. In fact, the thermal diffusivity can be about twice the momentum diffusivity of the free stream (homogeneous turbulence). The free stream turbulence at the entrance to the nozzle of the Lewis Research Center facility was observed to be close to 2 percent in intensity. Downstream in the nozzle this would be appreciably smaller - say about 1 percent. Nevertheless, this is an appreciable value, which suggests that the momentum diffusivity of the free stream. The time-averaged temperature profiles indicate a shape which is associated with a turbulent diffusivity in the outer region. As shown in figure 4, the slope of the outer portion is 1/7 or greater, which definitely denotes a turbulent eddy transport.

The Model and Laminarization

Although this report is directed at turbulent accelerating flow, the model of the thermal layer for this condition does appear to be extrapolable to the so-called relaminarization condition. This condition results from an acceleration history in the boundary layer. Under conditions of acceleration the viscous boundary layer appears to be stabilized and the net production of turbulent eddies is reduced. Profile studies of the accelerating turbulent velocity layer show that it tends to approach the character of a laminar boundary layer, (see refs. 6 and 13). Launder and Stinchcombe (ref. 13) have conjectured that acceleration inhibits the production of large eddies in the intermittent region of the boundary layer. These large eddies are the principal source of turbulence in the boundary layer. In our opinion, sufficient inhibition of large eddy production could lead to laminarization.

Turbulence intensity measurements (ref. 13) did show that although the time-averaged velocity profiles appeared laminar-like, a definite turbulent-like structure persists. Thus, labeling the phenomenon "laminarization" is somewhat misleading. The turbulent structure of the velocity boundary layer, although attenuated, does persist into the domain of laminar-like heat transfer levels.

Referring to the model of the thermal layer (fig. 6), shows that the stabilizing or laminarizing effects in the velocity layer would be sensed primarily in the near-wall region of the temperature boundary layer. Any changes in the local velocity gradient would alter the temperature gradient in this region.

However, stabilizing the velocity layer would inhibit the convection of turbulent eddies into the free stream. Conceivably, the loss, or reduction, of this source of turbulence

supply would tend to attenuate the level of turbulence in the free stream. As was pointed out in the previous section, the thermal eddy diffusivity is related to the level of momentum eddy diffusivity in the free stream. One would conclude then that the near-wall and free stream regions would both experience reduced turbulent heat transport when relaminarization of the velocity layer set in.

ANALYTICAL APPROACH

In reference 1, a simplified version of the integral energy equation was proposed. In the course of developing the final expression of the equation it was assumed that Stanton number was a function of the Reynolds number based on energy thickness. (The reader is referred to the appendix of ref. 1.) For the special case of an isothermal wall, constant viscosity and a perfect recovery factor the energy equation reduces to the simple form

$$Nu_r = 0.0143\, Re_{d,r}^{0.75}\, Pr_r \left(\frac{\varphi}{d}\right)^{-0.25} \tag{3a}$$

or, alternatively, for Stanton number

$$St_r = 0.0143\, Re_{d,r}^{-0.25} \left(\frac{\varphi}{d}\right)^{-0.25} \tag{3b}$$

From equation (3b) it is apparent that the Stanton number is a function of a Reynolds number in which the length dimension is energy thickness. To make use of this simplified energy equation, one must know the local energy thickness as well as the local flow Reynolds number. The latter can be approximated from the familiar one-dimensional flow equations. The evaluation of the energy thickness comes from the integration of the energy equation through the nozzle. In reference 1, it was shown that the energy thickness Reynolds number for an axi-symmetric flow nozzle could be computed from the following equation:

$$(Re_\varphi r)^{1.25} = 0.018 \int_{z=0}^{z} \frac{\rho_r}{\rho} \frac{(Re_{\varphi,r})^{-0.25}}{\varphi} (Re_\varphi r)^{1.25} \left[1 + \left(\frac{dr}{dz}\right)^2\right]^{1/2} dz + (Re_\varphi r)_{z=0}^{1.25} \tag{4}$$

This is a somewhat approximate version which pertains to a nozzle with an isothermal wall, where the recovery factor is one and where the viscosity is assumed constant. Generally, these approximations are applicable to a real rocket nozzle. Despite these simplifications, the use of equation (4) in design-type calculations is too complicated. Consequently, we would like to propose further simplifications which would enable local energy thickness estimates in the nozzle.

In this section we will present such a simplification to an estimation of the energy thickness or the energy thickness Reynolds number by considering a one-dimensional flow model. As a means of evaluating such a simplification, the computed energy thickness values will be compared with the experimental measurements (data presented in fig. 3). Then the computed values will be incorporated into equation (3b) to obtain heat transfer estimates. These heat-transfer estimates will be compared with measured rates and with the rates computed by inserting experimentally determined energy thicknesses into equation (3b). These cross comparisons will enable an evaluation of the prediction method in the light of heat transfer and thermal boundary layer data.

Finally, the prediction method will be applied to a variety of air and rocket nozzles. These nozzle tests representing a range of geometries, heat fluxes, and temperature ratios. The predicted Stanton number grouping will be compared with the measured parameter.

The detailed development of the equations will be presented in the appendix. Starting with the one-dimensional approximation to equation (4), namely,

$$Re_{\varphi}^{1.25} = C \int_{S=0}^{S} \frac{\rho u}{\mu} dS + Re_{\varphi_{S=0}}^{1.25} \tag{5}$$

it is shown in the appendix that the energy thickness can be estimated as the sum of two functions. One function represents the contribution to the energy thickness in the nozzle and the other represents the contribution made in the constant diameter inlet.

As is shown in the appendix, the approximate one-dimensional integration was done for three distinct regions: the constant diameter inlet, the nozzle convergent section, and the nozzle divergent section. The equations pertaining to each of these sections are now discussed.

For the constant diameter inlet section, the expression for the energy thickness is

$$\frac{\varphi}{d} = 0.0565 Re_d^{-0.2} Pr^{-0.6} \left(\frac{l}{d}\right)^{0.767} \tag{6}$$

The Reynolds number and Prandtl number are evaluated at bulk conditions.

The energy thickness in the convergent portion of the nozzle including the throat evolves from equation (5). The convergent section is approximated as a cone (curvature in the vicinity of the throat is neglected). When the effects of a variable viscosity are neglected, the expression for energy thickness at any station in the convergent section, including the throat, is

$$\frac{\varphi}{d} = \frac{1}{Re_d}\left\{0.0179\, d_{th}\, Re_{d,\,th}\, \frac{S}{d_i d} + \left[Re_d\left(\frac{\varphi}{d}\right)\right]_{S=0}^{1.25}\right\}^{0.8} + \frac{d_i}{d}\left\{2.43\times10^{-8}\left[Re_d\left(\frac{\varphi}{d}\right)\right]_{S=0}^{1.25} + 0.0005\right\} \tag{7}$$

Again, the fluid properties are evaluated at bulk conditions. As is discussed in the appendix, the second term in equation (7) represents an empirical adjustment to make the energy thickness agree more closely with the more complicated integral boundary layer method. This added term can be interpreted as an integration correction.

The energy thickness in the supersonic portion of the nozzle is estimated by extending the integration limits of equation (5) to include the divergent portion of the nozzle. The divergent section geometry is represented as a cone. The expression for energy thickness which is valid in the supersonic section only is

$$\frac{\varphi}{d} = \frac{1}{Re_d}\left\{0.0179 Re_{d,\,th}\left(\frac{S_{th}}{d_i} + \frac{\bar{S}}{d_{th}}\right) + \left[Re_d\left(\frac{\varphi}{d}\right)\right]_{S=0}^{1.25}\right\}^{0.8} + \frac{d_i}{d}\left\{2.43\times10^{-8}\left[Re_d\left(\frac{\varphi}{d}\right)\right]_{S=0}^{1.25} + 0.0005\right\} \tag{8}$$

Equations (6) to (8) are estimates for the energy thickness in the constant diameter section (chamber in a chemical rocket engine), the convergent section, and the divergent section. In figure 7, the estimated energy thickness based on these equations is compared to the actual measurements and to the more involved Bartz-type integral boundary layer method. These comparisons were carried out for both an adiabatic and cooled inlet upstream of the air nozzle.

It is apparent from the figure that the simplified method does a pretty good job of estimation in the convergent region and throat, but does a poor estimation in the diver-

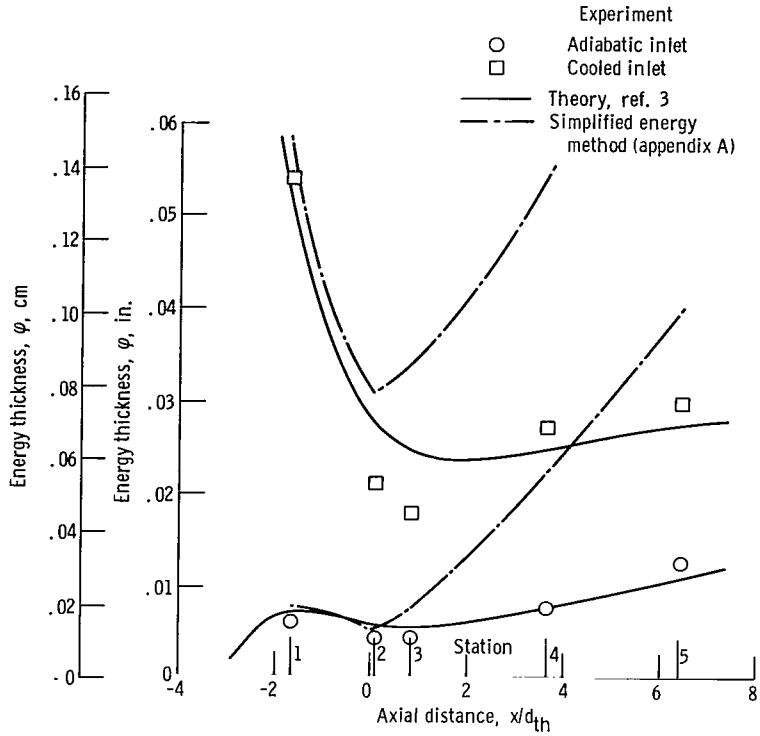

Figure 7. - Experimental and theoretical energy thickness distributions for tests with an adiabatic and cooled inlet. Free-stream total temperature, T_0, 970° R (539 K); throat diameter, d_{th}, 1.492 inches (3.790 cm).

gent portion. However, the simplified energy method is designed for the subsonic and sonic sections of the nozzle only, where the energy thickness greatly exceeds the momentum thickness (recall fig. 3). Thus, it is not surprising that the method does a poor job in the supersonic section of the nozzle.

It should be noted that the Bartz boundary layer method of reference 3 predicts the energy thickness quite accurately throughout the entire nozzle.

Comparison of Estimates to Experimental Heat Transfer

In these comparisons of the estimated heat transfer to the experimental values, we will first examine equation (3b) by inserting experimental values of energy thickness φ into the equation and comparing the computed heat transfer to the measured. Figures 8(a) and (b) are a comparison made for the throat and convergent instrument station (M = 0.08) cooled and adiabatic inlet. The data curves displayed are for a range of Reynolds numbers but the comparison applies to the high Reynolds numbers only. For the throat

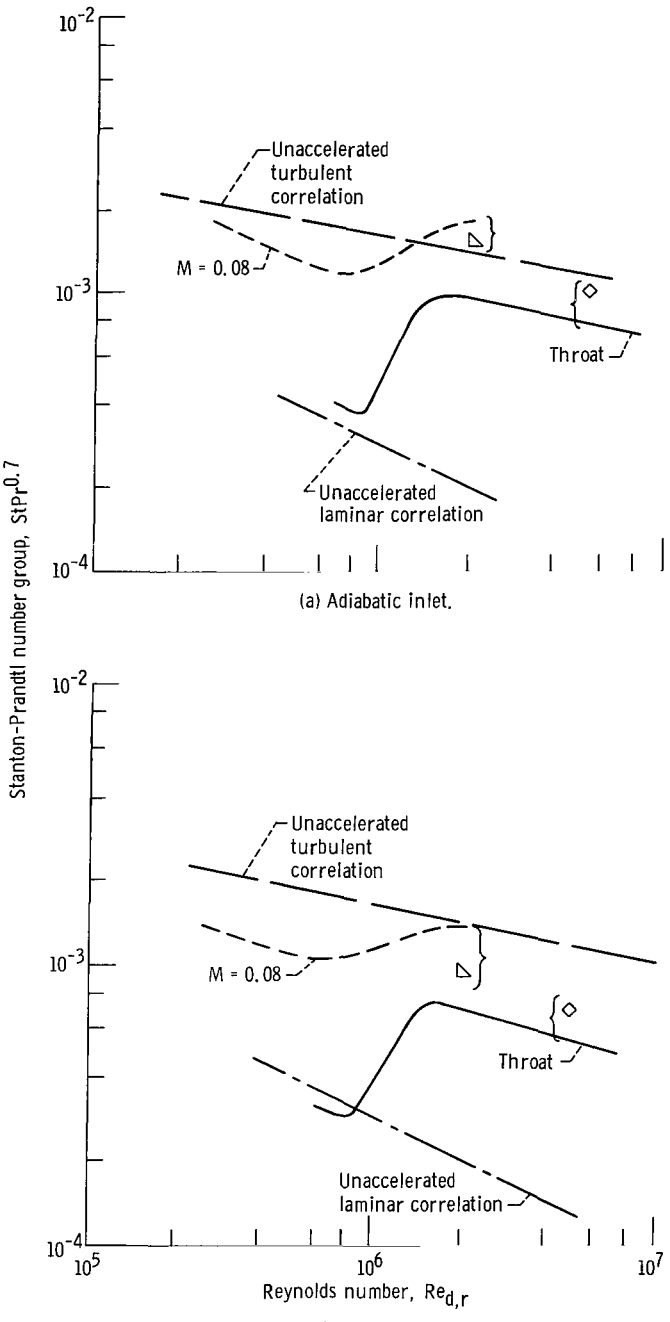

Figure 8. - Comparison of computed heat transfer (based on experimental energy thickness) to experimental heat transfer. Inlet diameter, 6.5 inches (0.165 m). Curves are loci of experimental points.

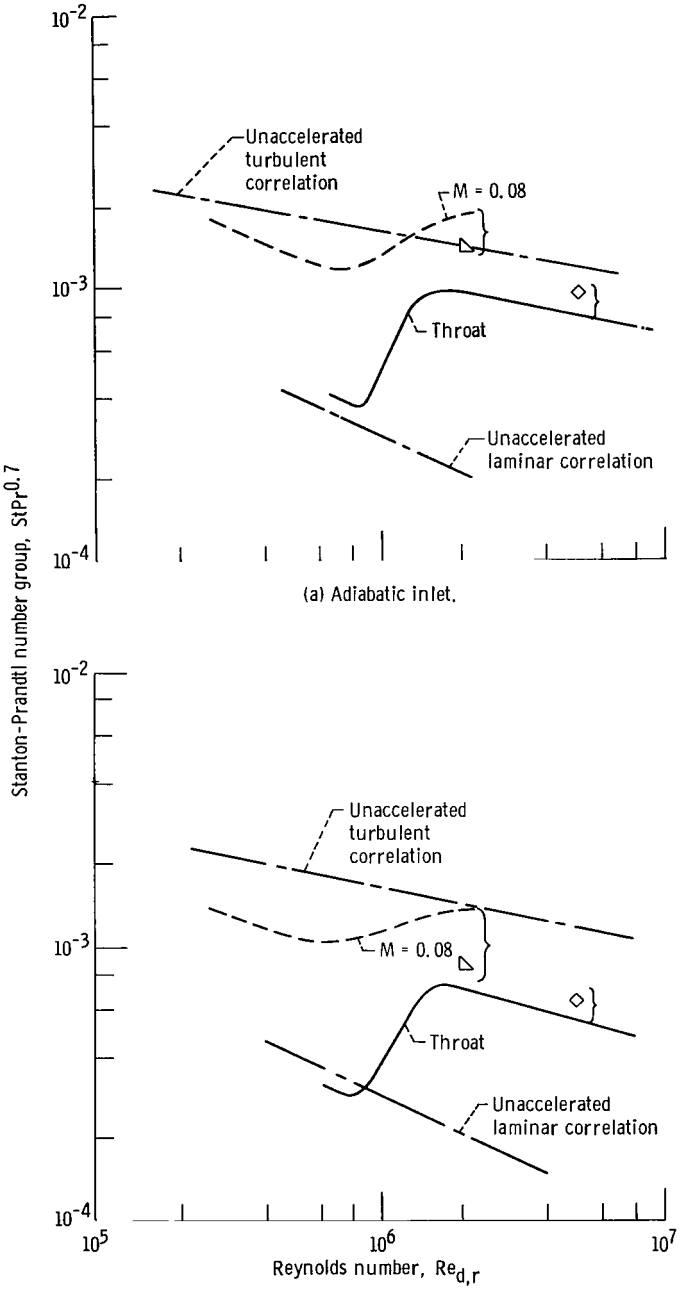

Figure 9. - Comparison of computed heat transfer (based on computed energy thickness) to experimental heat transfer. Inlet diameter, 6.5 inches (0.165 m).

station the predicted heat transfer is high by 20 or 25 percent. However, for the $M = 0.08$ station, the computed is low by 20 to 50 percent. But note that the experimental heat transfer is high at this station when compared to the nonaccelerated turbulent correlation. This is particularly noticeable for the case of the adiabatic inlet. This elevated level of heat transfer is ascribed to curvature effects and temperature step (adiabatic inlet only). From figures 8(a) and (b), one can conclude that the integral energy prediction by equation (3b) is fairly accurate at the throat. It is a decided improvement over the nonaccelerated turbulent correlation.

In the comparisons that follow, the energy thickness will be estimated at the throat station by use of equation (7). The Stanton number will be estimated by inserting that energy thickness along with the appropriate Reynolds number into equation (3b).

Figures 9(a) and (b) are essentially a repetition of figures 8(a) and (b) except that the computed points were obtained as mentioned in the previous paragraph. The estimates are quite close to what was obtained by inserting experimental energy thicknesses into equation (3b). This is not surprising because it was shown earlier (fig. 7) that equation (7) predicted the experimental energy thicknesses at the throat quite accurately.

Next, the method was applied to the throat of one of the JPL air nozzle configurations. The line in figure 10 was faired through the experimental data taken at the throat station. The point symbol represents the estimated value using the simplified method and the agreement is very close.

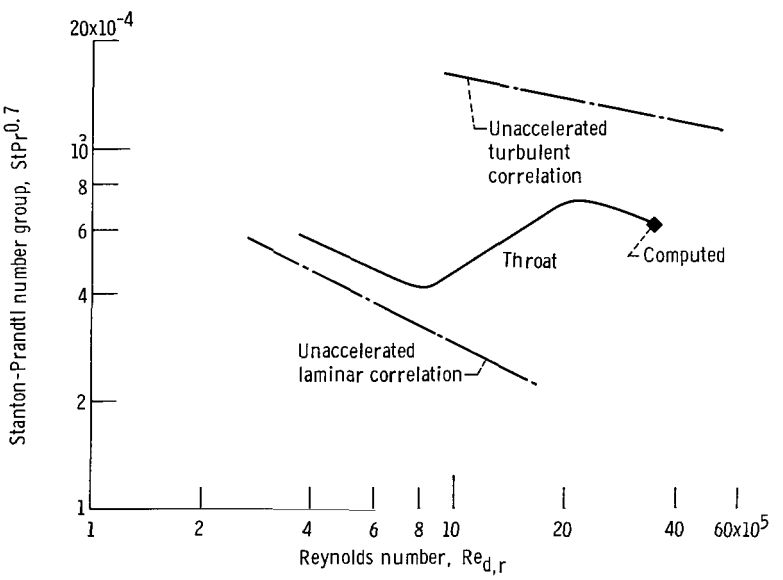

Figure 10. - Comparison of simple energy method to data of reference 14 (properties adjusted to reference temperature). Free-stream total temperature, T_0, 1500° R (833 K); 45° half-angle of convergence nozzle; wall to free stream temperature ratio, T_w/T_0, 0.5.

The ability of the method to comprehend contraction ratio was disappointing. Figures 11(a) and (b) relate to the Lewis nozzle facility. The lines in these figures are fairings of the experimental data. For both nozzle geometries it is to be noted that the estimate of the Stanton number for cooled inlet is very low at the small contraction ratio. The other estimated points are generally within a respectable tolerance. Certainly, for both the cooled and adiabatic inlets, the estimates do not agree with the trends of the experimental data (slope) with the contraction ratio. In fact, with the cooled inlet the trend is opposite to that of experiment.

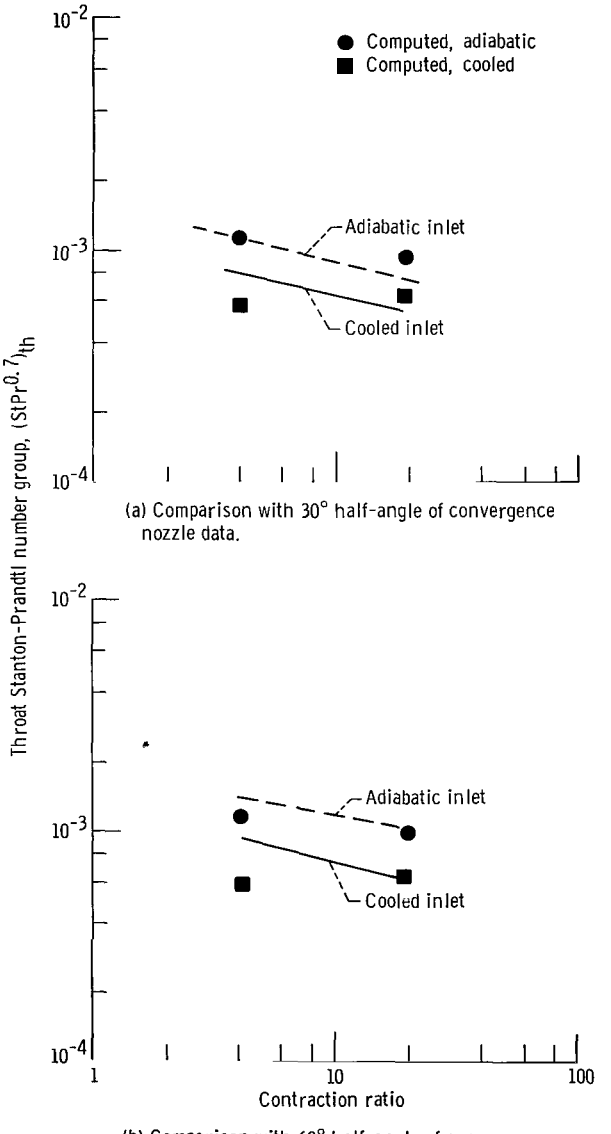

(a) Comparison with 30° half-angle of convergence nozzle data.

(b) Comparison with 60° half-angle of convergence nozzle data.

Figure 11. - Evaluation of simple integral method. Wall to free-stream total temperature ratio, T_w/T_0, 0.85.

The method has been compared to tests with two chemical rocket nozzle configurations. Both utilized a hydrogen-oxygen propellant combination. Figure 12(a) is the Stanton-Prandtl group as a function of Reynolds number for the nozzle which had an area contraction ratio of 4.7. The lower line on the graph is the average of the experimental data taken from reference 7. The nonaccelerated correlation locus is also shown. The estimate at a Reynolds number of 5×10^6 is close to the average of the experimental data.

Figure 12(b) is some unpublished heat transfer data (obtained from W. L. Jones of Lewis) for a hydrogen-oxygen chemical rocket with an area contraction ratio of 12. Because relatively few experimental data points are involved, they are shown as open circles. The solid diamond is the computed Stanton-Prandtl parameter that corresponds to a Reynolds number of 3 million. The estimate is low. However, the experimental data appear to exhibit two levels. More data runs, now being analyzed, may allow a more defined locus of experimental data.

For both the heated air and rocket heat transfer results, the energy methods appear to predict the throat heat transfer satisfactorily.

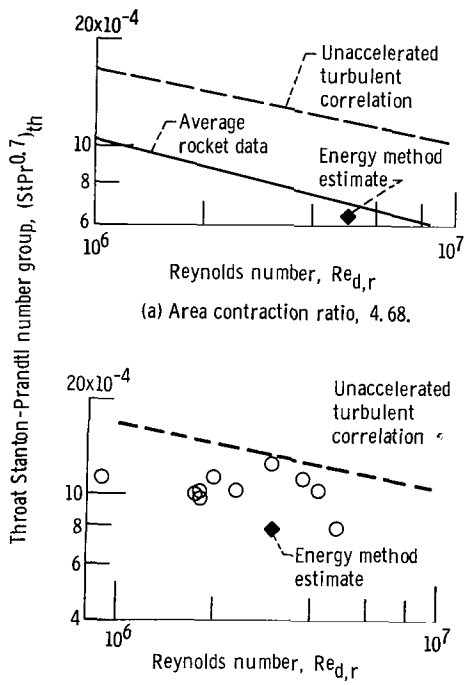

Figure 12. - Evaluation of simple integral method. Comparison to hydrogen-oxygen rocket; wall to free-stream total temperature ratio, T_w/T_0, 0.25.

SUMMARY REMARKS

Measurements in the turbulent boundary layer of the convergent portion of a convergent-divergent nozzle have verified that the thermal layer is much thicker than the velocity layer. Consequently, a logical model of the boundary layer would involve a two-layer description. Near the wall, the eddy transport mechanism would be controlled by the turbulence of the velocity layer. In the outer region, the eddy transport is governed by the free stream turbulence. The eddy transport of both layers is attenuated by acceleration in the nozzle.

In an integral boundary layer approach for predicting the throat heat transfer, neglecting the velocity layer thickness appears to be a satisfactory approximation. Integral thermal layer thicknesses measured at the throat were inserted into a simplified integral analysis (ref. 1) and it was found that the computed heat transfer approximated the measured values for several geometries.

The relative success of the integral energy method led to the establishment of a calculational procedure in which the energy thickness at the throat of any nozzle geometry can be estimated. After the energy thickness is estimated, it is a comparatively simple matter to compute the throat heat transfer from the hot gas into the wall. The applicability of the method was tested on several nozzle configurations including two chemical rockets, and the comparison of measurement to prediction was favorable.

Lewis Research Center,
National Aeronautics and Space Administration,
Cleveland, Ohio, May 7, 1969,
129-01-05-19-22.

APPENDIX - CALCULATION OF ENERGY THICKNESS

Energy Thickness in Pipe Inlet

In many rocket nozzle configurations the converging portion of the nozzle is preceded by a short entrance section similar to a pipe. The thermal boundary layer generally does not have sufficient length to become fully developed. It is well known that the heat transfer in short pipes exceeds the value for fully developed flow. Therefore, the calculation of energy thickness in the pipe inlet will be based on heat transfer data in the entrance regions of tubes. The air data of reference 15 have been selected for this analysis. A good approximation of the ratio of local-to-fully developed heat transfer (Stanton number) for these data is

$$\frac{St}{St_{fd}} = 1.88 \left(\frac{l}{d}\right)^{-0.233} \tag{A1}$$

The Stanton number for fully developed flow can be expressed as

$$St_{fd} = 0.023\, Re_d^{-0.2} Pr^{-0.6} \tag{A2}$$

Substitution of equation (A2) into equation (A1) and introduction of the integral energy equation for unit Prandtl number and an isothermal wall yield

$$St = 0.0433\, Re_d^{-0.2} Pr^{-0.6} \left(\frac{l}{d}\right)^{-0.233} = \varphi \frac{d}{dl} \ln \rho u \varphi \tag{A3}$$

or

$$\int_{\varphi=0}^{\varphi} \varphi \, d \ln \rho u \varphi = 0.0433 \int_{l=0}^{l} Re_d^{-0.2} Pr^{-0.6} \left(\frac{l}{d}\right)^{-0.233} dl \tag{A4}$$

Equation (A4) can be readily integrated assuming constant properties and the boundary condition $\varphi(0) = 0$ to yield the following expression for φ/d:

$$\frac{\varphi}{d} = 0.0565\, Re_d^{-0.2} Pr^{-0.6} \left(\frac{l}{d}\right)^{0.767} \tag{A5}$$

Since the constant in equation (A1) was based on the establishment of fully developed flow at $l/d = 15$, equation (A5) is valid in the range of $0 \leq l/d \leq 15$. This length-to-diameter ratio should be adequate for the majority of present day rocket nozzle configurations.

Energy Thickness in the Subsonic Nozzle

Examination of the expression for the energy thickness in a nozzle, given in reference 1, suggests that the local energy thickness is strongly dependent on the integrated mass flux. Therefore, the energy thickness Reynolds number can be approximated by an expression of the following type (see eq. (A5) of ref. 1):

$$Re_\varphi^{1.25} = 0.0179 \int_{S=0}^{S} \frac{\rho u}{\mu}\, dS + Re_{\varphi_{S=0}}^{1.25} \tag{A6}$$

The mass flux ρu will be approximated by the following expression:

$$\rho u = 0.532 \frac{P_0}{\sqrt{T_0}} \frac{A_{th}}{A} \tag{A7}$$

Substitution of equation (A7) into equation (A6) with the assumption of constant viscosity yields

$$Re_\varphi^{1.25} = 0.0179\, d_{th}\, Re_{d,\,th} \int_{S=0}^{S} \frac{dS}{d^2} + Re_{\varphi_{S=0}}^{1.25} \tag{A8}$$

The integral in equation (A8) can be evaluated in closed form if the subsonic portion of the nozzle is approximated by a truncated cone as shown in figure 13.

The integral in equation (A8) can be expressed as

$$\int_{S=0}^{S} \frac{dS}{d^2} = \int_{S=0}^{S} \frac{dS}{(d_i - 2S \sin \alpha)^2} = \frac{S}{d_i d} \tag{A9}$$

Substitution of equation (A9) into equation (A8) and rearranging yield the following first-order expression for φ/d:

$$\frac{\varphi}{d} = \frac{1}{Re_d} \left\{ 0.0179\, d_{th}\, Re_{d,\,th}\, \frac{S}{d_i d} + \left[Re_d \left(\frac{\varphi}{d} \right) \right]_{S=0}^{1.25} \right\}^{0.8} \tag{A10}$$

The values of energy thickness based on equation (A10) were less than predictions based on the theory of reference 2. Results from the latter analysis are in good agreement with

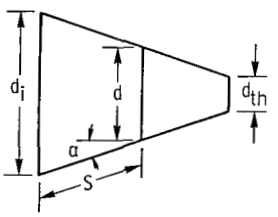

Figure 13. - Cone approximation of subsonic nozzle.

the data as shown in figure 7. In order to account for the difference between the results of the two methods, it was necessary to empirically weight the inlet function. Upon applying inlet correction factor, the final expression for φ/d is

$$\frac{\varphi}{d} = \frac{1}{Re_d} \left\{ 0.0179\, d_{th}\, Re_{d,\,th}\, \frac{S}{d_i d} + \left[Re_d \left(\frac{\varphi}{d} \right) \right]_{S=0}^{1.25} \right\}^{0.8} + \frac{d_i}{d} \left\{ 2.43 \times 10^{-8} \left[Re_d \left(\frac{\varphi}{d} \right) \right]_{S=0}^{1.25} + 0.0005 \right\} \tag{A11}$$

The predictions of φ based on equation (A11) are in good agreement with the results of reference 3 as shown in figure 7 ($x/d_{th} \leq 0$).

Energy Thickness in the Supersonic Nozzle

The previous analysis can be extended to the supersonic portion of the nozzle by assuming the nozzle effuser can be represented by a truncated cone. This is depicted in figure 14. In supersonic flow it is necessary to extend the limits of the integral in equation (A8) in accordance with the assumed cone approximations. The resulting integral becomes

$$\int_{S=0}^{S_{th}+\bar{S}} \frac{dS}{d^2} = \left(\frac{S_{th}}{d_i d_{th}} + \frac{\bar{S}}{d_{th} d}\right) \tag{A12}$$

Substitution of this expression into equation (A11) yields the following relations for φ/d, valid for $x/d_{th} > 0$:

$$\frac{\varphi}{d} = \frac{1}{Re_d}\left\{0.0179\, Re_{d,th}\left(\frac{S_{th}}{d_i} + \frac{\bar{S}}{d}\right) + \left[Re_d\left(\frac{\varphi}{d}\right)\right]_{S=0}^{1.25}\right\}^{0.8}$$

$$+ \frac{d_i}{d}\left\{2.43\times10^{-8}\left[Re_d\left(\frac{\varphi}{d}\right)\right]_{S=0}^{1.25} + 0.0005\right\} \tag{A13}$$

The distributions of energy thickness based on equation (A13) rapidly diverge from the results based on the theory of reference 3 (refer to fig. 7). The pronounced over prediction of energy thickness, especially at the downstream end of the nozzle, suggest that the method be restricted to the vicinity of the throat. However, this limitation on the applicability of the method does not pose serious problems with respect to heat transfer calculations since the heat transfer energy thickness relation is valid only in this throat region.

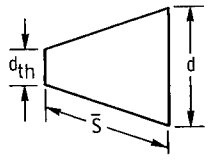

Figure 14. - Cone approximation of supersonic nozzle.

REFERENCES

1. Boldman, Donald R.; Neumann, Harvey E.; and Schmidt, James F.: Heat Transfer in 30° and 60° Half-Angle of Convergence Nozzles With Various Diameter Uncooled Pipe Inlets. NASA TN D-4177, 1967.

2. Boldman, D. R.; Schmidt, J. F.; and Ehlers, R. C.: Effect of Uncooled Inlet Length and Nozzle Convergence Angle on the Turbulent Boundary Layer and Heat-Transfer in Conical Nozzles Operating With Air. J. Heat Transfer, vol. 89, no. 4, 1967, pp. 341-350.

3. Elliot, David G.; Bartz, Donald R.; and Silver, Sidney: Calculation of Turbulent Boundary-Layer Growth and Heat-Transfer in Axi-Symmetric Nozzles. Tech Rep. 32-387, Jet Propulsion Lab., California Inst. Tech., 1963.

4. Siegel, Robert; and Sparrow, E. M.: Simultaneous Development of Velocity and Temperature Distributions in a Flat Duct with Uniform Wall Heating. AIChE J., vol. 5, no. 1, Mar. 1959, pp. 73-75.

5. Kays, W. M.: Convective Heat and Mass Transfer. McGraw-Hill Book Co., Inc., 1966, pp. 118-120.

6. Boldman, Donald R.; Schmidt, James F.; and Gallagher, Anne K.: Laminarization of a Turbulent Boundary Layer as Observed From Heat-Transfer and Boundary-Layer Measurements in Conical Nozzles. NASA TN D-4788, 1968.

7. Schacht, Ralph L.; Quentmeyer, Richard J.; and Jones, William L.: Experimental Investigation of Hot-Gas Side Heat-Transfer Rates for a Hydrogen-Oxygen Rocket. NASA TN D-2832, 1965.

8. Back, L. H.; and Witte, A. B.: Prediction of Heat Transfer From Laminar Boundary Layers with Emphasis on Large Free-Stream Velocity Gradients and Highly Cooled Walls. Tech. Rep. 32-728, Jet Propulsion Lab., California Inst. Tech. (NASA CR-63904), June 1, 1965.

9. Moretti, P. M.; and Kays, W. M.: Heat Transfer Through an Incompressible Turbulent Boundary Layer With Varying Free-Stream Velocity and Varying Surface Temperature. Rep. PG-1, Thermosciences Div., Mech. Eng. Dept., Stanford Univ., Nov. 1964.

10. Back, L. H.; Massier, P. F.; and Cuffel, R. F.: Some Observations on Reduction of Turbulent Boundary-Layer Heat Transfer in Nozzles. AIAA J., vol. 4, no. 12, Dec. 1966, pp. 2226-2229.

11. Deissler, Robert G.: Weak Locally Homogeneous Turbulence and Heat Transfer With Combined Two-Dimensional Shear and Normal Strain. NASA TN D-4273, 1967.

12. Graham, R. W.; and Deissler, R. G.: Prediction of Flow-Acceleration Effects on Turbulent Heat Transfer. J. Heat Transfer, vol. 89, no. 4, Nov. 1967, pp. 371-372.

13. Launder, B. E.; and Stinchcombe, H. S.: Non-Normal Similar Turbulent Boundary Layers. Rep. TWF/TN/21, Mech. Eng. Dept., Imperial College of Science and Technology, London, May 1967.

14. Back, L. H.; Massier, P. F.; and Cuffel, R. F.: Flow Phenomena and Convective Heat Transfer in a Conical Supersonic Nozzle. J. Spacecraft Rockets, vol. 4, no. 8, Aug. 1967, pp. 1040-1047.

15. Boelter, L. M. K.; Young, G.; and Iversen, H. W.: An Investigation of Aircraft Heaters. XXVII - Distribution of Heat-Transfer Rate in the Entrance Section of a Circular Tube. NACA TN 1451, 1948.

NASA-Langley, 1969 —— 33 E-5076

NATIONAL AERONAUTICS AND SPACE ADMINISTRATION
WASHINGTON, D. C. 20546
OFFICIAL BUSINESS

FIRST CLASS MAIL

POSTAGE AND FEES PAID
NATIONAL AERONAUTICS AND
SPACE ADMINISTRATION

POSTMASTER: If Undeliverable (Section 158 Postal Manual) Do Not Return

"The aeronautical and space activities of the United States shall be conducted so as to contribute . . . to the expansion of human knowledge of phenomena in the atmosphere and space. The Administration shall provide for the widest practicable and appropriate dissemination of information concerning its activities and the results thereof."

—NATIONAL AERONAUTICS AND SPACE ACT OF 1958

NASA SCIENTIFIC AND TECHNICAL PUBLICATIONS

TECHNICAL REPORTS: Scientific and technical information considered important, complete, and a lasting contribution to existing knowledge.

TECHNICAL NOTES: Information less broad in scope but nevertheless of importance as a contribution to existing knowledge.

TECHNICAL MEMORANDUMS: Information receiving limited distribution because of preliminary data, security classification, or other reasons.

CONTRACTOR REPORTS: Scientific and technical information generated under a NASA contract or grant and considered an important contribution to existing knowledge.

TECHNICAL TRANSLATIONS: Information published in a foreign language considered to merit NASA distribution in English.

SPECIAL PUBLICATIONS: Information derived from or of value to NASA activities. Publications include conference proceedings, monographs, data compilations, handbooks, sourcebooks, and special bibliographies.

TECHNOLOGY UTILIZATION PUBLICATIONS: Information on technology used by NASA that may be of particular interest in commercial and other non-aerospace applications. Publications include Tech Briefs, Technology Utilization Reports and Notes, and Technology Surveys.

Details on the availability of these publications may be obtained from:

SCIENTIFIC AND TECHNICAL INFORMATION DIVISION

NATIONAL AERONAUTICS AND SPACE ADMINISTRATION

Washington, D.C. 20546